

# Chemical composition, crystal size and lattice structural changes after incorporation of strontium into biomimetic apatite

Z.Y. Li<sup>a</sup>, W.M. Lam<sup>a</sup>, C. Yang<sup>b</sup>, B. Xu<sup>b</sup>, G.X. Ni<sup>a</sup>, S.A. Abbah<sup>a</sup>, K.M.C. Cheung<sup>a</sup>,  
K.D.K. Luk<sup>a</sup>, W.W. Lu<sup>a,\*</sup>

<sup>a</sup>Department of Orthopaedics and Traumatology, The University of Hong Kong, Hong Kong, China

<sup>b</sup>Department of Chemistry, Hong Kong University of Science and Technology, Hong Kong, China

Received 11 September 2006; accepted 1 November 2006  
Available online 30 November 2006

## Abstract

Recently, strontium (Sr) as ranelate compound has become increasingly popular in the treatment of osteoporosis. However, the lattice structure of bone crystal after Sr incorporation is yet to be extensively reported. In this study, we synthesized strontium-substituted hydroxyapatite (Sr-HA) with different Sr content (0.3%, 1.5% and 15% Sr-HA in mole ratio) to simulate bone crystals incorporated with Sr. The changes in chemical composition and lattice structure of apatite after synthetic incorporation of Sr were evaluated to gain insight into bone crystal changes after incorporation of Sr. X-ray diffraction (XRD) patterns revealed that 0.3% and 1.5% Sr-HA exhibited single phase spectrum, which was similar to that of HA. However, 15% Sr-HA induced the incorporation of  $\text{HPO}_4^{2-}$  and more  $\text{CO}_3^{2-}$ , the crystallinity reduced dramatically. Transmission electron microscopy (TEM) images showed that the crystal length and width of 0.3% and 1.5% Sr-HA increased slightly. Meanwhile, the length and width distribution were broadened and the aspect ratio decreased from  $10.68 \pm 4.00$  to  $7.28 \pm 2.80$ . The crystal size and crystallinity of 15% Sr-HA dropped rapidly, which may suggest that the fundamental crystal structure is changed. The findings from this work indicate that current clinical dosage which usually results in Sr incorporation of below 1.5% may not change chemical composition and lattice structure of bone, while it will broaden the bone crystal size distribution and strengthen the bone.

© 2006 Elsevier Ltd. All rights reserved.

**Keywords:** Bone crystal; Strontium-substituted; Hydroxyapatite; Nanocrystallite

## 1. Introduction

Strontium (Sr) is a trace element that is found in calcareous rocks and ocean water. It is also a natural component of food and beverages. Based on the element's ability to enhance bone volume [1,2] and prevent bone loss [3,4], Sr has become increasingly popular in the prevention and treatment of osteoporosis as a ranelate compound [5–7]. Sr has been associated with improving postmenopausal osteoporosis by reducing bone resorption and increasing bone formation with an eventual effect of

decreasing the risk of fractures [8]. In vitro studies revealed that strontium ranelate (SR) has an anabolic and antiresorptive activity which leads to an increase in both the collagen and non-collagen protein synthesis, an enhancement in pre-osteoblast differentiation, an inhibition in osteoclast differentiation, and a reduction in osteoclast function [9].

In line with its chemical analogy to calcium (Ca), Sr is a bone seeking element and 98% of the total body Sr content can be found in the skeleton. After the administration of Sr salt for the prevention or treatment of osteoporosis, Sr passes through the Haversian capillaries walls by diffusion to reach the bone extracellular fluid and finally deposit in the bone being absorbed on the bone apatite surface or substitute the Ca positions in bone crystal [10].

Boivin et al. [11,12] studied the biodistribution of Sr by X-ray microanalysis after oral administration of SR to

\*Corresponding author. Department of Orthopaedics and Traumatology, Room 907, Lab Block, 21 Sassoon Road, The University of Hong Kong, Hong Kong. Tel.: +852 2819 9595 or 2974 0332; fax: +852 2818 5210.

E-mail address: [wlu@hkusua.hku.hk](mailto:wlu@hkusua.hku.hk) (W.W. Lu).

monkeys. Changes at the bone crystal level were evaluated with X-ray diffraction (XRD) and Raman microspectroscopy. The results indicated that the content of Sr in both cortical and cancellous bone in the treated group was higher than that of the control but induced no major modifications of bone mineral at the crystal level. In osteoporotic monkeys treated with the highest dose of 750 mg SR/kg/day, bone Sr-content may increase to level of 1.2 mol% Sr/Ca [11]. However, the amount of Sr in human body is only 0.02 mol% of Ca. The Sr in bone after SR treatment was 60 times more than that in normal level. The ionic radius of Sr ion (1.13 Å) is higher than that of the Ca ion (0.99 Å). With the incorporation of Sr in bone crystal, the distance of Sr-hydroxyl will be greater than that of Ca-hydroxyl. Consequently, decreases in lattice energy (cohesion is inversely proportional to the distance) and, therefore, in crystallinity are possible. Thus, the Sr incorporation in bone mineral may lead to the modifications in lattice parameters, in crystal size, and in the crystallinity of bone mineral [11].

As the mechanical strength of both cortical and trabecular bone is related to the crystal size, crystallinity and composition of bone crystal [13], changes in the chemical composition of bone crystal could account for changes in the mechanical strength of both cortical and trabecular bone. But no detailed information has been reported about the effects of Sr incorporation on composition and crystal structure of bone crystal after Sr incorporation. Due to the similarity to basic mineral phase of human bone and teeth and containing other ions in addition to Ca and P [14], synthesis of chemically modified or ion-substituted hydroxyapatite (HA) has drawn interest from many scientists [15–21]. Since it has been suggested that the interaction of Sr with bone is similar to that with synthetic HA [22,23], Sr substituted HA was also used to simulate the bone crystal with Sr incorporation and the effects of Sr on bone mineral content and bone mineral density were determined [24]. It is well known that at the nanoscale level, the main basic mineral phase of bone crystal is nano-hydroxyapatite. So Sr substituted hydroxyapatite (Sr-HA) nanocrystallite were synthesized to simulate bone crystal with Sr incorporation in the present study. Based on pilot studies, Sr-HA with different Sr concentrations were synthesized. The purpose of this study was to examine the effects of Sr incorporation on chemical composition, crystal size, crystallinity and lattice structure of Sr-HA nanocrystallite.

## 2. Materials and methods

### 2.1. Preparation of Sr-HA

$\text{Ca}(\text{NO}_3)_2 \cdot 4\text{H}_2\text{O}$ ,  $\text{Sr}(\text{NO}_3)_2$  and  $(\text{NH}_4)_2\text{HPO}_4$  were used as the Ca, Sr and P sources, respectively. Sr-HA nanocrystallite with different Sr content were synthesized by replacing  $\text{Ca}(\text{NO}_3)_2 \cdot 4\text{H}_2\text{O}$  with  $\text{Sr}(\text{NO}_3)_2$ . Commercially available analytical grade (AR)  $\text{Ca}(\text{NO}_3)_2 \cdot 4\text{H}_2\text{O}$ ,  $\text{Sr}(\text{NO}_3)_2$  and  $(\text{NH}_4)_2\text{HPO}_4$  were used with the molar ratio of 10:6, which was the desired Ca/P ratio observed in HA.

$\text{Ca}(\text{NO}_3)_2 \cdot 4\text{H}_2\text{O}/\text{Sr}(\text{NO}_3)_2$  and  $(\text{NH}_4)_2\text{HPO}_4$  were dissolved in distilled water with the concentration of 0.2 M. The pH value of the solutions was adjusted to 10 by adding 25% ammonia solution. Then,  $(\text{NH}_4)_2\text{HPO}_4$  solution was added dropwise into the  $\text{Ca}(\text{NO}_3)_2/\text{Sr}(\text{NO}_3)_2$  mixture solution by syringe pump (Razel Scientific Instruments, Inc., CT, USA) at 2.8 ml/h with 400 rpm stirring at 50 °C. The pH value of the reaction solution was kept at 10 by the addition of ammonia solution. When finished dropping, the solution was kept stirring at 400 rpm and aging at 50 °C for 5 h. Subsequently, the precipitate was filtered, it was washed several times with distilled water and absolute ethanol. The product was placed in an oven and heated at 120 °C for 12 h for drying.

### 2.2. Characterization techniques

The atomic concentrations of elements (Ca and Sr) in the samples were quantified by X-ray Fluorescence (XRF) method on a JEOL JSX-3201Z Element Analyzer. Samples were prepared using the borate fusion method, where 0.1–0.5 g of sample is fused into a glass disc with 5 g of lithium tetraborate/lithium metaborate (50/50). The limit of quantification (LOQ) for all the elements examined in this work is 0.001 mol%.

In order to examine the chemical composition of Sr-HA, FT-IR was performed to study the powder using a typical KBr pellet technique. The Sr-HA powder was grounded with KBr in the proportion of 1/150 (by weight) and pressed into a 3 mm pellet using a hand press. The FT-IR spectrum was collected using Perkin-Elmer Spectrum One FTIR Spectrometer (PerkinElmer, USA) in the range 4000–400  $\text{cm}^{-1}$ .

Phase analysis of the synthesized HA and Sr-HA powders was conducted using primarily XRD employing a Philips Powder X-ray diffractometer PW1830 (Philips Analytic, Netherlands) using Cu K radiation ( $\lambda = 1.5418 \text{ \AA}$ ) equipped with a Si detector. The diffractometer was operated at 45 kV and 40 mA at a  $2\theta$  range of 10–50° employing a step size of 0.05 and a 50 s exposure. Crystallographic identification of the Sr-HA was accomplished by comparing the experimental XRD patterns to standards compiled by the Joint Committee on Powder Diffraction and Standards (JCPDS; HA, card #09-0432).

TEM images were taken on a TEM Tecnai 20 (Philips Analytic, Netherlands) microscope at 200 kV. High-resolution imaging (HRTEM) and selected-area electron diffraction (SAED) patterns were obtained on single crystal.

### 2.3. Determination of crystal size and crystallinity of Sr-HA

The size of individual Sr-HA crystallites were calculated from XRD data using the Scherrer equation and verified by measuring 200 particles by TEM. The peak of 25.9°  $2\theta$  (0 0 2) was fit to define its full width at half maximum intensity ( $B_{1/2}(\text{rad}-2\theta)$ ):

$$d = \frac{k\lambda}{B_{1/2} \cos \theta} \quad (1)$$

where  $d$  is the crystal size, as calculated for the ( $hkl$ ) reflection,  $\lambda$  is the wavelength of Cu K $_{\alpha}$  radiation ( $\lambda = 1.5418 \text{ \AA}$ ), and  $k$  is the broadening constant varying with crystal habit and chosen as 0.9 for the elongated apatite crystallites.

The crystallinity noted by  $X_c$ , corresponds to the fraction of crystalline apatite phase in the investigated volume of powdered sample. An empirical relation between  $X_c$  and the  $B_{1/2}$  was deduced, according to the equation as below:

$$B_{1/2} \times \sqrt[3]{X_c} = K_A \quad (2)$$

where  $X_c$  is the crystallinity degree,  $B_{1/2}$  is the full width of the peak at half intensity of (0 0 2) reflection in (degree- $2\theta$ ),  $K_A$  is a constant set at 0.24.

Possible changes in the crystal structure (lattice parameters) were quantified. Interplanar distances ( $d$  values) obtained by XRD (peak 25–27° = 002 planes; peak 30–35° = 211 + 300 planes; peak 39–40° = 310 planes) allowed the calculation of the parameters  $a$  and  $c$  from the crystal

lattice following the Eqs. (3) and (4):

$$\lambda = 2d_{hkl} \sin \theta_{hkl} \quad (3)$$

$$\frac{1}{d_{hkl}^2} = \frac{4}{3} \left( \frac{h^2 + hk + l^2}{a^2} \right) + \frac{l^2}{c^2} \quad (4)$$

#### 2.4. Evaluation of size distribution by TEM

Crystal shape and size distribution were analyzed by transmission electron microscopy (TEM) for comparison with XRD calculated result. The analyzing procedure implies taking an area domain from a microscopic image and counting the total number of particles using

$$N_t = \sum_i N_i, \quad (5)$$

where  $N_t$  express the total number of particles while  $N_i$  is the number of fraction 'i', with the same features, either particle length, width or aspect ratio. The percentage of each population with the same characteristic features can be calculated accordingly:

$$F(\%) = \frac{N_i}{\sum_i N_i} \times 100. \quad (6)$$

$F$  represents the fraction number, expressed as percentage (%).

#### 2.5. Data analysis

Dedicated softwares such as DigitalMicrograph 365 (for PC) (Gatan, Inc., Pleasanton, CA) and MicroCall Origin provided image processing and mathematical data computation. Data were expressed as mean  $\pm$  SD unless otherwise stated. For each of the various study parameters, the various study groups (i.e., different Sr incorporation) vs. the control group (HA) were compared by ANOVA. The criterion for statistical significance was  $p < 0.05$ .

### 3. Results

#### 3.1. Chemical analysis

The compositions of the powders examined by XRF are summarized in Table 1. All of the measurements are within uncertainty of the expected compositions. At the beginning of this work, we expected the preparation of HA without Sr incorporation and no Sr salt was added in starting materials. It was not surprising that HA had a measured Sr content of 0.02%. Traceable Sr in water and other sources may incorporate in HA during the reaction. In addition, the Sr content in HA was similar to the normal level in human body. 0.3%, 1.5% and 15% Sr-HA were obtained

Table 1  
Expected and measured elemental composition of Sr-HA

Sample	Expected Sr/(Ca + Sr)%	XRF results		
		Ca (mol%)	Sr(mol%)	Sr/(Ca + Sr)%
HA	0	68.237	0.016	0.02
Sr-HA	0.3	67.274	0.209	0.31
	1.5	67.101	1.068	1.57
	15	55.413	10.031	15.33

to simulate the bone crystal with 15, 75 and 750 times Sr than that in normal bone.

FT-IR spectra of Sr-HA nanocrystallite were shown in Fig. 1. The absorption bands at 1044( $v_3$ ), 962( $v_1$ ), 566( $v_4$ ) and 475( $v_2$ ) detected in the spectrum, which were attributed to the phosphate ( $\text{PO}_4^{3-}$ ) characteristic absorption, were presented in all spectra for the synthetic apatites. But at 15% Sr incorporation, markedly broadened peaks in both the 1044( $v_3$ ) and 566( $v_4$ ) domain were observed (Fig. 1d). When Sr incorporation was or above 1.5%, carbonate absorption bands were observed at around 1484–1421  $\text{cm}^{-1}$ . This absorption intensity was strengthened with the increased incorporation of Sr. The absorption bands at 875 and 1885  $\text{cm}^{-1}$  were assigned to the hydrogen phosphate ( $\text{HPO}_4^{2-}$ ), which was detected at 15% Sr incorporation (Fig. 1d). But it was not observed in other Sr-HA.

The typical XRD patterns of all Sr-HA were shown in Fig. 2. 1.5% and less Sr incorporation did not markedly change the patterns of Sr-HA (Fig. 2b and c). Upon Sr incorporation with atomic ratio 15%, the peak of (002) was dramatically broadened and shifted towards smaller angle numbers. The peaks at  $2\theta$  range from 28° to 29° and 31° to 34° were overlapped, respectively (Fig. 2d).

#### 3.2. Crystal size, crystallinity and lattice parameters reflected from the XRD pattern

For quantitative purposes, the line broadening of the (002) reflection was used to evaluate the mean crystallite size. It is due to the fact that this peak is well resolved and shows no interferences. The  $d_{002}$  values are related to crystal size in the wide dimension of the HA crystallites. The average width and their corresponding crystallinity of

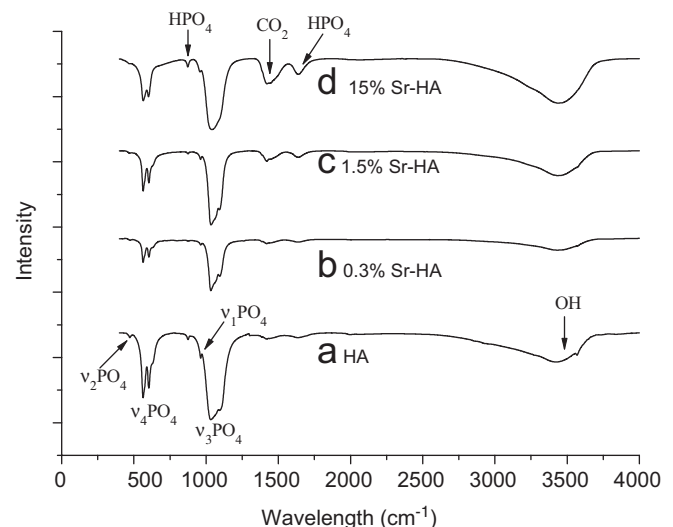


Fig. 1. FT-IR spectra of HA (a) and Sr-HA (b–d) with different Sr incorporation. Phosphate characteristic absorptions were presented in all spectra. 15% Sr substitution induced the incorporation of  $\text{HPO}_4^{2-}$  and more  $\text{CO}_3^{2-}$ .

Sr-HA crystallite were calculated, as shown in Table 2. The  $d_{002}$  value of HA and 0.3–1.5% Sr-HA were 23.31 nm. However, the size decreased considerably to 12.54 nm when the powder was incorporated by 15% Sr. A reduction in synthetic Sr-HA crystal size at comparable Sr-concentrations was also previously reported by Christoffersen et al. [24]. The change of crystallinity on Sr-HA was similar to that of crystal size. The dramatically decreased crystallinity and size of 15% Sr-HA were confirmed by TEM results, as presented in Figs. 3 and 4.

The cell parameters of the samples are shown in Table 3. The space group of HA and Sr-HA is  $P6_3/m$ . The lattice parameters for both  $a$  and  $c$  slightly increased when Ca ions are replaced by Sr in the HA framework.

### 3.3. Crystallinity, lattice structure and crystal size of Sr-HA

In order to confirm the XRD results concerning the size and crystallinity of Sr-HA, TEM measurements were performed. A similar observation was revealed by SAED

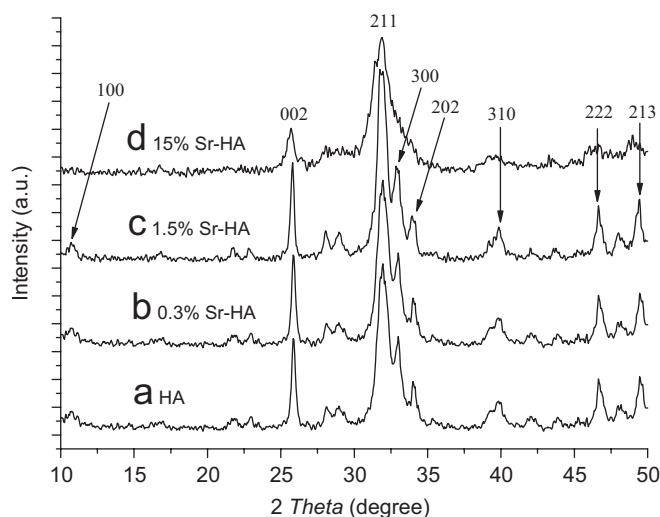


Fig. 2. XRD patterns of HA (a) and Sr-HA (b–d) with different Sr incorporation. 1.5% and less Sr incorporation did not change the patterns of Sr-HA, while the peaks of 15% Sr-HA were broadened.

Table 2  
Crystal size and crystallinity of Sr-HA reflected by XRD pattern

Sample	Line width (002) FWHM, (rad)	Average crystal size $d$ (nm) by Scherrer's equation	Line width (002) FWHM, (deg)	Crystallinity ( $X_c$ )
HA	0.0061	23.31	0.35	0.3224
Sr-HA				
0.3%	0.0061	23.31	0.35	0.3224
1.5%	0.0061	23.31	0.35	0.3224
15%	0.0113	12.54	0.65	0.0503

FWHM: full-width at half-maximum intensity of peak (002).

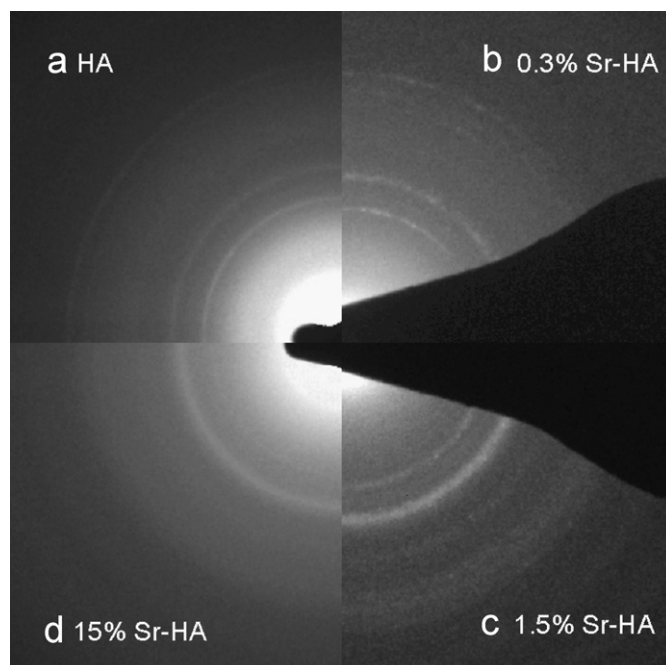


Fig. 3. SAED patterns of Sr-HA with different Sr incorporation. The crystallinity of Sr-HA doped with 0.3% and 1.5% Sr were comparable with that of HA, while a diffuse background was observed in the SAED pattern of 15% Sr-HA.

(Fig. 3) when compared with XRD analysis (Fig. 2). Here the crystallinity of Sr-HA doped with 0.3% and 1.5% Sr were comparable with that of HA. But a diffuse background was observed in the SAED pattern of 15% Sr-HA, indicating a reduced crystallinity and/or the presence of an amorphous phase. The results of SAED were consistent with the results of XRD, both of which revealed the decreased crystallinity after 15% Sr incorporation in HA.

Fig. 4a(Left) shows the TEM micrographs together with HRTEM patterns for the HA crystals. Well-defined nano-crystallites of HA in the range of 50–150 nm can be seen in the TEM image. Fig. 4a(Right) showed the HRTEM image recorded from the crystals of the individual HA nano-needle shown in Fig. 4a(Left). The regular spacing of the observed lattice planes was about 0.35 nm, which was consistent with the (002) lattice spacing of HA.

Below 1.5% Sr-HA, the morphological change with minimum change in crystal size was not considerable (Fig. 4b and c). The HRTEM image and SAED results indicated that crystallinity of Sr-HA did not change, however the crystal size increased slightly. From the TEM examination of Sr-HA (15%), we could see that the crystals melt together (Fig. 4d). HRTEM images also showed that the (002) lattice spacing of 0.3% and 1.5% Sr-HA were uniformly 0.34 nm, which was similar to the (002) lattice spacing of HA. However, the poor crystallinity of 15% Sr-HA prevents an accurate determination of the lattice spacing values. The observed lattice spacing of 15% Sr-HA was 0.28 nm.

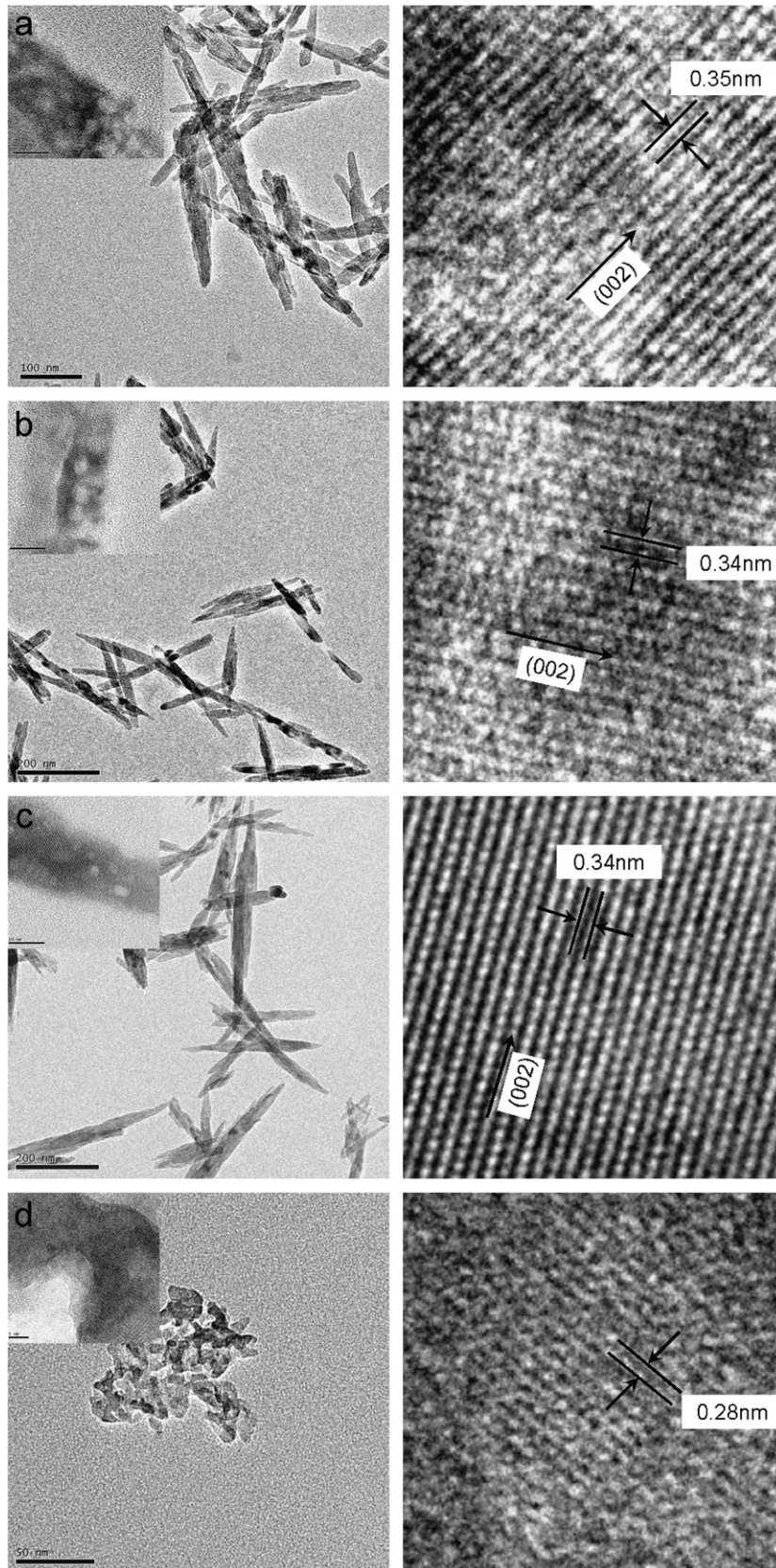


Fig. 4. (a) TEM (Left) and HRTEM (Right) of HA; (b) TEM (Left) and HRTEM (Right) of 0.3% Sr-HA; (c) TEM (Left) and HRTEM (Right) of 1.5% Sr-HA; (d) TEM (Left) and HRTEM (Right) of 15% Sr-HA; 1.5% and less Sr incorporation did not change the crystal shape and lattice spacing of Sr-HA (a–c). However, the crystal size and observed lattice spacing dramatically decreased with 15% Sr incorporation (d).

Table 3  
Lattice parameters of Sr-HA

Sample	Space group	Lattice parameters
HA	$P6_3/m$	$a = 9.3689 \text{ \AA}$ , $c = 6.8798 \text{ \AA}$
Sr-HA	0.3%	$a = 9.3825 \text{ \AA}$ , $c = 6.8929 \text{ \AA}$
	1.5%	$a = 9.3997 \text{ \AA}$ , $c = 6.9060 \text{ \AA}$
	15%	$a = 9.4252 \text{ \AA}$ , $c = 6.9591 \text{ \AA}$

The TEM micrographs, displayed in Fig. 4 were used to calculate the distribution of length, width and aspect ratio of Sr-HA. By shape, the Sr-HA were found to be needle-like. Because of the aggregation problem with 15% Sr-HA, we only collected the data of the below 1.5% Sr-HA. The length, width and aspect ratio distribution of Sr-HA are shown in Fig. 5. The length and width of Sr-HA were found to be between 50–600 nm and 5–50 nm, respectively. Although there was no considerable difference between the average length of HA and Sr-HA (Table 4), the distribution peaks of HA were narrow while the distribution peak became broader with the increasing of Sr incorporation (Fig. 5a). Similar results were observed with width distribution (Fig. 5b). However, the aspect ratio of the

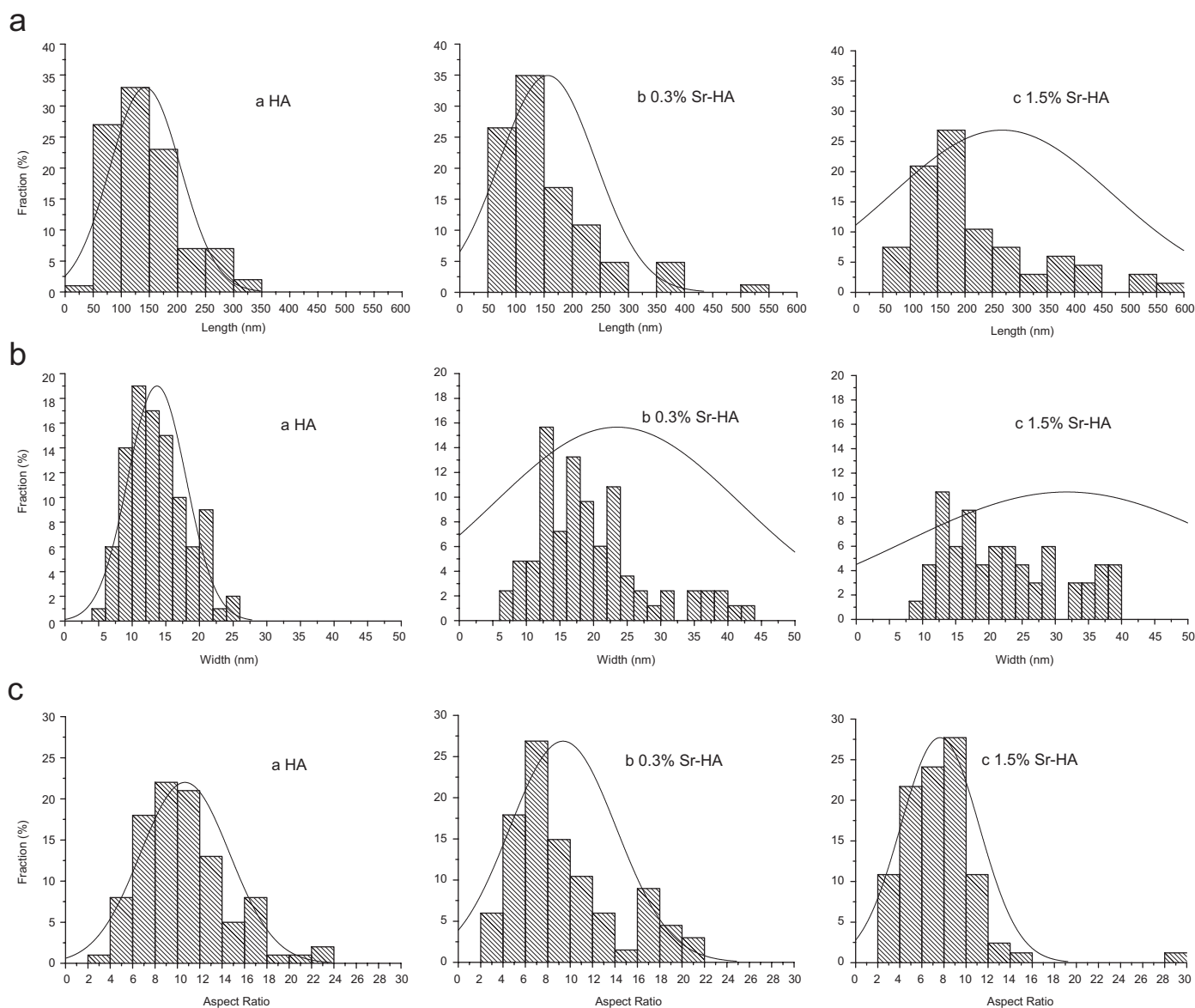


Fig. 5. (a) Length distribution of HA and Sr-HA; (b) width distribution of HA and Sr-HA; (c) aspect ratio distribution of HA and Sr-HA. There was no considerable difference between the average length and width of HA and Sr-HA, while the distribution of length and width was broadened (a and b). The aspect ratio decreased dramatically with the Sr incorporation (c).

Table 4  
Crystal size of Sr-HA evaluated by TEM

Sample	Height (nm)	Width (nm)	Aspect ratio
HA	142.6 ± 63.2	14.86 ± 4.34	10.68 ± 4.00
Sr-HA			
0.3%	168.1 ± 55.0	18.15 ± 10.90	9.37 ± 4.77
1.5%	152.2 ± 54.7	19.83 ± 8.64	7.28 ± 2.80*

Control: HA; \**p*-value < 0.05.

nanocrystallite decreased significantly with the Sr incorporation (Fig. 5c).

#### 4. Discussion

In this study, Sr-HA was synthesized to simulate the bone crystal with Sr incorporation. The characteristic absorption of  $\text{PO}_4^{3-}$  revealed the presence of HA. The carbonate absorption bands indicated that carbonate ions had substituted for certain phosphate positions in the apatite lattice (B-type substitution) [25,26]. In precipitated biological apatites, the predominant substitution appears to be  $\text{CO}_3^{2-}$  ions for  $\text{PO}_4^{3-}$  ions, but usually a small amount of  $\text{OH}^-$  ion replacement (A-type substitution) also occurs [27]. The carbonate substitution may be due to the reactive absorption of atmospheric carbon dioxide by the alkaline solution during the slurry preparation and reaction. The carbonate substitution was more obvious when 15% of the Ca was substituted by Sr. It was possibly because of the larger structural strain caused by partial substitution of Sr for Ca, which suggested that the Sr-HA can accommodate more carbonate ions into its structure [28]. The  $\text{HPO}_4^{2-}$  group appeared to be substituted for the  $\text{PO}_4^{3-}$  group in the crystals after 15% Sr incorporation. As Guerra et al. explained for nickel ions [29], it is likely that Ca for Sr substitution favors  $\text{HPO}_4^{2-}$  incorporation. This also was observed in Kikuchi's study [30]. So we considered that insufficient positive charge was because the cation deficiency was compensated by substitution of the  $\text{HPO}_4^{2-}$  group for the  $\text{PO}_4^{3-}$  group. More carbonate ions incorporation and the broadening peaks in both 1044( $v_3$ ) and 566( $v_4$ ) domain indicated a reduced crystallinity of Sr-HA and it was confirmed by the XRD results described below.

The XRD results indicated that the Sr incorporation at atomic ration lower than 1.5% did not impact the crystallinity of Sr-HA. However, 15% Sr incorporation broadened the XRD peaks (Fig. 2d). The broadening of the X-ray line width indicated that the incorporation of Sr destroyed the symmetry. The substitution of Sr for Ca produces a distortion in the phosphate environment. The further Sr incorporation may decrease the crystallinity and restrain the growth of Sr-HA as nickel [29].

The ionic radius of Sr (1.13 Å) is larger than the one of Ca (0.99 Å), which is in agreement with the observed increase in lattice parameters for Sr-HA. The change of the

lattice parameters of Sr-HA clearly demonstrated that Sr ion was structurally incorporated, in other words, they did not just cover the surface of crystal.

The crystal size collected from TEM indicated that Sr incorporation increased the length and width slightly, but decreased the aspect ratio (Table 4). Though the data about 15% Sr-HA was not collected, the TEM morphology showed unambiguously that the size was decreased dramatically (Fig. 4d). Although the size evaluated by TEM was smaller than that reflected by XRD patterns, the changing trend of crystal size after Sr incorporation was consistent with the result calculated from XRD pattern (Table 2). Some similar results were previously reported in Verberckmoes's experiment [31].

Comparable average size with broadened distribution (Fig. 5a and b) after low (below 1.5%) Sr incorporation is not necessarily an adverse effect. Since it is suggested by others that the bone crystal size distribution becomes sharper, bone tends to fracture more easily [13]. Hence, broadening in the bone crystal size distribution can be one of the explanations of the observed increase of bone strength in Sr-treated osteoporosis patients.

All the results in the present study, including those reflected from XRD and evaluated by TEM, indicated that below 1.5% Sr-HA did not change the crystal structure while increased the crystal size slightly. However, 15% Sr incorporation dramatically decreased the crystal size and crystallinity. The changes in crystal size and crystallinity of Sr-HA may be due to the  $\text{Sr}^{2+}$  substitution style of  $\text{Ca}^{2+}$ . The HA crystal structure shows two inequivalent  $\text{Ca}^{2+}$  sites (Fig. 6). Cations at site I, CaI, are coordinated by nine oxygens belonging to six  $\text{PO}_4^{3-}$  forming triangles and

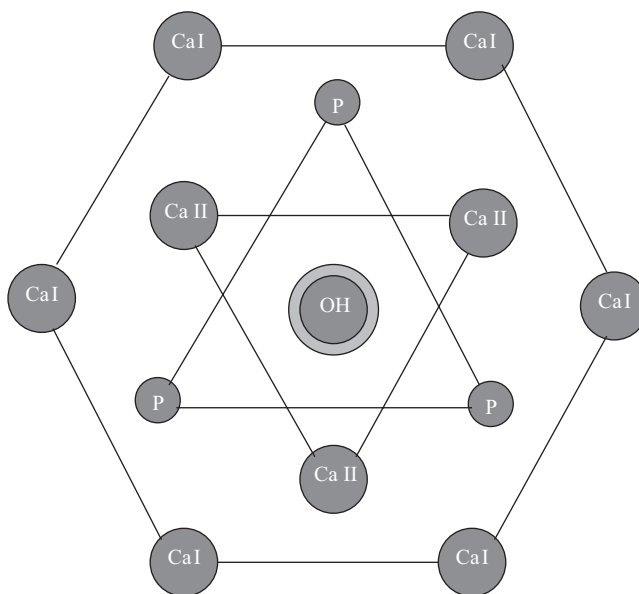


Fig. 6. The sketch of crystal structure of hydroxyapatite. The crystal structure shows two inequivalent Ca sites, CaI and CaII. Sr is incorporated preferentially at CaII. 0.3% and 1.5% incorporation of Sr expand the structural size of Sr-HA, while 15% Sr incorporation may have a destabilizing effect on the apatite structure.

displaying a columnar arrangement. Cations at site II are heptacoordinated by six oxygen atoms belonging to five  $\text{PO}_4^{3-}$  anions and one  $\text{OH}^-$  anion. The smallest distance between a cation and a coordinated oxygen is found at site II, while the smallest Ca–Ca distances are observed between  $\text{Ca}^{2+}$  ions at site I [32]. Small ions (such as  $\text{Cd}^{2+}$ ,  $\text{Zn}^{2+}$  and  $\text{Mg}^{2+}$ ) are incorporated preferentially in the HA structure at CaI [33]. In contrast, large cations (such as  $\text{Sr}^{2+}$ ,  $\text{Ba}^{2+}$  and  $\text{Pb}^{2+}$ ) would first replace  $\text{Ca}^{2+}$  at CaII. In the present case, Sr ions were substituted preferentially at the CaII site. Because the ionic radius of Sr (1.13 Å) is larger than the one of Ca (0.99 Å), 0.3% and 1.5% incorporation of Sr expand the structural size of Sr-HA, which induced the slight increase in length and width of Sr-HA. However, 15% Sr incorporation may have a destabilizing effect on the apatite structure, which destroyed the symmetry and produced a distortion in the phosphate environment [29]. The more  $\text{CO}_3^{2-}$  and  $\text{HPO}_4^{2-}$  incorporation also changed the crystal composition of Sr-HA and induced a loss of crystallinity. The changes on crystal structure and composition with Sr incorporation may change the crystal growth mechanism and restrain the growth of the crystal. The crystal growth of HA preferred the long axis (001) direction [34]. Broadened size distribution and decreased aspect ratio might indicate that Sr incorporation inhibited the growth of the crystal along the long axis direction, which was confirmed further by the decreasing size of 15% Sr-HA.

The total amount of Sr (about 320 mg in human body [35]) in the skeleton is small compared to Ca. In osteoporotic patients treated with current clinical dosage of 2 g SR/day, femur and lumbar vertebra Sr content is below 1.5 mol% Sr/(Sr+Ca) [36]. Based on this present experiment and results, we can evaluate the changes in bone crystal with Sr incorporation. Natural bone crystal is structurally related to the synthesized hydroxyapatite, but the inclusion of vacancies and impurities (e.g.,  $\text{Mg}^{2+}$ ,  $\text{Sr}^{2+}$ ,  $\text{CO}_3^{2-}$ ,  $\text{HPO}_4^{2-}$ , etc.) in the bone crystal lattice makes it different from synthesized crystal. More studies, such as to synthesize crystal under simulated body condition or use bone biopsies of patients with Sr treatment, should be performed to further elucidate the effects of Sr incorporation on bone crystal in the near future.

## 5. Conclusion

Below 1.5% Sr incorporation did not change the chemical composition and crystallinity of Sr-HA. Crystal length and width increased slightly with the Sr incorporation, while the size distribution broadened considerably. This information can be one of the explanations of the observed increase of bone strength in Sr-treated osteoporosis patients. However, 15% Sr incorporation dramatically decreased the crystal size and crystallinity, which may attribute to the destabilizing effect after more Sr incorporation. The information obtained in this work could suggest that Sr administration with current dosage

for prevention and treatment of osteoporosis will not change the composition and crystallinity of bone crystal, but more studies should be performed to further elucidate the effects of Sr incorporation on bone mineral.

## Acknowledgment

This study was partially supported by the University of Hong Kong Strategic Research Area Fund on Biomedical Engineering and Hong Kong ITF Fund JFS/064/05. The authors thank Mr. Hubert Tseng (The Johns Hopkins University, USA) for his assistance in improvement of English language for this manuscript.

## References

- [1] Delannoy P, Bazot D, Marie PJ. Long-term treatment with strontium ranelate increases vertebral bone mass without deleterious effect in mice. *Metabolism* 2002;51:906–11.
- [2] Blake GM, Fogelman I. Long-term effect of strontium ranelate treatment on BMD. *J Bone Miner Res* 2005;20:1901–4.
- [3] Takahashi N, Sasaki T, Tsouderos Y, Suda T. S 12911-2 inhibits osteoclastic bone resorption in vitro. *J Bone Miner Res* 2003;18:1082–7.
- [4] Hott M, Deloffre P, Tsouderos Y, Marie PJ. S12911-2 reduces bone loss induced by short-term immobilization in rats. *Bone* 2003;33:115–23.
- [5] El-Hajj Fuleihan G. Strontium ranelate—a novel therapy for osteoporosis or a permutation of the same? *N Engl J Med* 2004;350:504–6.
- [6] Meunier PJ, Roux C, Seeman E, Ortolani S, Badurski JE, Spector TD, et al. The effects of strontium ranelate on the risk of vertebral fracture in women with postmenopausal osteoporosis. *N Engl J Med* 2004;350:459–68.
- [7] Compston J. Prevention of vertebral fractures by strontium ranelate in postmenopausal women with osteoporosis. *Osteoporos Int* 2005;16:S4–6.
- [8] Marie PJ. Strontium ranelate: a physiological approach for optimizing bone formation and resorption. *Bone* 2006;38:S10–4.
- [9] Kendler DL. Strontium ranelate—data on vertebral and nonvertebral fracture efficacy and safety: mechanism of action. *Curr Osteoporos Rep* 2006;4:34–9.
- [10] Davies DR, Bassingthwaite JB, Kelly PJ. Transcapillary exchange of strontium and sucrose in canine tibia. *J Appl Physiol* 1976;40:17–22.
- [11] Boivin G, Deloffre P, Perrat B, Panczer G, Boudeulle M, Mauras Y, et al. Strontium distribution and interactions with bone mineral in monkey iliac bone after strontium salt (S 12911) administration. *J Bone Miner Res* 1996;11:1302–11.
- [12] Farlay D, Boivin G, Panczer G, Lalande A, Meunier PJ. Long-term strontium ranelate administration in monkeys preserves characteristics of bone mineral crystals and degree of mineralization of bone. *J Bone Miner Res* 2005;20:1569–78.
- [13] Adele B. Bone mineral crystal size. *Osteoporos Int* 2003;14:16–21.
- [14] Glimcher MG. The nature of the mineral phase in bone. San Diego, 1997. p. 23–50.
- [15] Skrtic D, Antonucci JM, Eanes ED, Brunworth RT. Silica- and zirconia-hybridized amorphous calcium phosphate: Effect on transformation to hydroxyapatite. *J Biomed Mater Res* 2002;59:597–604.
- [16] Bertoni E, Bigi A, Cojazzi G, Gandolfi M, Panzavolta S, Roveri N. Nanocrystals of magnesium and fluoride substituted hydroxyapatite. *J Inorg Biochem* 1998;72:29–35.
- [17] Mayer I, Featherstone JDB. Dissolution studies of Zn-containing carbonated hydroxyapatites. *J Cryst Growth* 2000;219:98–101.

- [18] Landi E, Tampieri A, Mattioli-Belmonte M, Celotti G, Sandri M, Gigante A, et al. Biomimetic Mg- and Mg<sub>2</sub>CO<sub>3</sub>-substituted hydroxyapatites: Synthesis, characterization and in vitro behaviour. *J Eur Ceram Soc* 2006;26:2593–601.
- [19] Coreno AJ, Coreno AO, Cruz R JJ, Rodriguez CC. Mechanochemical synthesis of nanocrystalline carbonate-substituted hydroxyapatite. *Opt Mater* 2005;27:1281–5.
- [20] Kim SR, Lee JH, Kim YT, Riu DH, Jung SJ, Lee YJ, et al. Synthesis of Si, Mg substituted hydroxyapatites and their sintering behaviors. *Biomaterials* 2003;24:1389–98.
- [21] Suchanek WL, Byrappa K, Shuk P, Riman RE, Janas VF, TenHuisen KS. Preparation of magnesium-substituted hydroxyapatite powders by the mechanochemical-hydrothermal method. *Biomaterials* 2004;25:4647–57.
- [22] Mac DN, Ezmirlan F, Spain P, Mc AC. The ultimate site of skeletal deposition of strontium and lead. *J Biol Chem* 1951;189:387–99.
- [23] Neuman WF, Bjornerstedt R, Mulryan BJ. Synthetic hydroxy apatite crystals. II. Aging and strontium incorporation. *Arch Biochem Biophys* 1963;101:215–24.
- [24] Christoffersen J, Christoffersen MR, Kolthoff N, Barenholdt O. Effects of strontium ions on growth and dissolution of hydroxyapatite and on bone mineral detection. *Bone* 1997;20:47–54.
- [25] Barralet J, Best S, Bonfield W. Carbonate substitution in precipitated hydroxyapatite: an investigation into the effects of reaction temperature and bicarbonate ion concentration. *J Biomed Mater Res* 1998;41:79–86.
- [26] Hing KA, Best SM, Bonfield W. Characterization of porous hydroxyapatite. *J Mater Sci-Mater Med* 1999;10:135–45.
- [27] Wilson RM, Dowker SEP, Elliott JC. Rietveld refinements and spectroscopic structural studies of a Na-free carbonate apatite made by hydrolysis of monetite. *Biomaterials* 2006;27:4682–92.
- [28] Kanno T, Horiuchi J-I, Kobayashi M, Motogami Y, Akazawa T. Characteristics of the carbonate ions incorporated into calcium-, partially-strontium-substituted and strontium apatites. *J Mater Sci Lett* 1999;18:1343–5.
- [29] Guerra-López J, Pomés R, Della Védova CO, Viña R, Punte G. Influence of nickel on hydroxyapatite crystallization. *J Raman Spectrosc* 2001;32:255–61.
- [30] Kikuchi M, Yamazaki A, Otsuka R. Crystal structure of Sr-substituted hydroxyapatite synthesized by hydrothermal method. *J Solid State Chem* 1994;113:373–8.
- [31] Verberckmoes SC, Behets GJ, Oste L, Bervoets AR, Lamberts LV, Drakopoulos M, et al. Effects of strontium on the physicochemical characteristics of hydroxyapatite. *Calcif Tissue Int* 2004;75:405–15.
- [32] Terpstra RA, Driessens FC. Magnesium in tooth enamel and synthetic apatites. *Calcif Tissue Int* 1986;39:348–54.
- [33] Baravelli S, Bigi A, Ripamonti A, Roveri N, Foresti E. Thermal behavior of bone and synthetic hydroxyapatites submitted to magnesium interaction in aqueous medium. *J Inorg Biochem* 1984;20:1–12.
- [34] Liu JB, Li KW, Wang H, Zhu MK, Xu HY, Yan H. Self-assembly of hydroxyapatite nanostructures by microwave irradiation. *Nanotechnology* 2005;16:82–7.
- [35] Pors Nielsen S. The biological role of strontium. *Bone* 2004;35:583–8.
- [36] Dahl SG, Allain P, Marie PJ, Mauras Y, Boivin G, Ammann P, et al. Incorporation and distribution of strontium in bone. *Bone* 2001;28:446–53.